Eur. Phys. J. C (2022) 82:453
https://doi.org/10.1140/epjc/s10052-022-10305-0

THE EUROPEAN PHYSICAL JOURNAL C

Regular Article - Theoretical Physics

Impact of a thermal medium on newly observed $Z_{cs}(3985)$ resonance and its b-partner

J. Y. Süngü[1,a], **A. Türkan**[2], **H. Sundu**[1], **E. Veli Veliev**[1]

[1] Department of Physics, Kocaeli University, 41001 Izmit, Turkey
[2] Department of Natural and Mathematical Sciences, Özyeğin University, Çekmeköy, Istanbul, Turkey

Received: 30 November 2020 / Accepted: 11 April 2022 / Published online: 17 May 2022

Abstract Motivated by the very recent discovery of the strange hidden-charm exotic state $Z_{cs}(3985)$ by the BESIII Collaboration, we study the possible interpretation of this exotic state the both at $T = 0$ and $T \neq 0$. We analytically compute the mass and meson-current coupling constant of this resonance with spin-parity $J^P = 1^+$ at finite temperature approximation up to the sixth order of the thermal operator dimension including non-perturbative contributions. Extracting thermal mass and meson-current coupling constant sum rules, the modifications on properties of the $Z_{cs}(3985)$ state in hot medium are determined. As a by-product, the hadronic parameters of the bottom partner of $Z_{cs}(3985)$ is estimated as well. The search for temperature effects on the hadronic parameters of the hidden-charm meson $Z_{cs}(3985)$ and the bottom partner enable us to understand the phase transitions, chiral symmetry breaking, and the properties of hot-dense matter in QCD. Moreover, the full width of the resonance $Z_{cs}(3985)$ is calculated as (12.0 ± 0.8) MeV using the strong decay in the tetraquark picture. Results for width and mass are in reasonable agreement with existing experimental data and results of other theoretical works. The information obtained about the parameters of the considered states is useful for experimental investigations of exotic mesons.

1 Introduction

Although many new exotic states, called XYZ states, above the $D\overline{D}$ threshold have recently been observed in different experiments, their substructures cannot yet be clearly explained. There are many candidates for exotic hadrons in the charmonium sector of quantum chromodynamics (QCD) studied in vacuum, hot medium, and in nuclear medium, such as $X(3872)$, $Z_c(3900)$, $Z_c(4430)$, $Y(4260)$, $Z_b(10610)$, and $Z_b'(10650)$ [1–13] which opens a new horizon for understanding the inner structure of strongly interacting matter. Investigating charged charmonium-like states is one of the most promising ways of searching for exotic mesons, since they must contain at least four quarks and thus cannot be a conventional hadron.

Recently, the BESIII Collaboration reported for the first time a charged strange hidden charmonium-like structure $Z_{cs}(3985)$ near the $D_s^- D^{*0}$ and $D_s^{*-} D^0$ mass thresholds in the K^+ recoil-mass spectrum for events collected at $\sqrt{s} = 4.681$ GeV in the processes of $e^+e^- \to K^+(D_s^- D^{*0} + D_s^{*-} D^0)$ [14]. The significance was estimated to be 5.3σ. This discovery could offer some unique hints to uncover the secrets of charged exotic Z structures. This new hadronic structure is assigned to the class of exotic state as the strange partner of $Z_c(3900)$ and studied in many different models in the literature in the molecular and tetraquark scenarios [15–25]. Its mass and width are defined in experiment as

$$\begin{aligned} M_{Z_{cs}} &= 3982.5^{+1.8}_{-2.6} \pm 2.1 \text{ MeV}, \\ \Gamma_{Z_{cs}} &= 12.8^{+5.3}_{-4.4} \pm 3.0 \text{ MeV}. \end{aligned} \tag{1}$$

Meanwhile, the features of matter under extreme conditions of high temperature and/or density have attracted the curiosity of high-energy physicists [26–30]. QCD, the theory of strong interactions, expects that nuclear matter undergoes a phase transition from a state of deconfined quarks and gluons, forming a new state of matter, called quark–gluon plasma (QGP), at a critical temperature $T_c \cong 155$ MeV ($\sim 10^{12}$ K) [31–34], which is in excellent agreement with the freeze-out temperature for hadrons measured by the ALICE collaboration at the Large Hadron Collider (LHC), producing ^{4}He and $^4\overline{\text{He}}$ nuclei in Pb–Pb collisions at $\sqrt{s_{NN}} = 2.76$ TeV in the rapidity range $|y| < 1$ [35,36]. Nevertheless, its short lifetime (10 fm/$c \approx 3 \times 10^{-23}$ s) and thermalization time (0.2 fm/$c \approx 7 \times 10^{-25}$ s), which make measurements harder, are a considerable challenge for experimentalists.

[a] e-mail: jyilmazkaya@kocaeli.edu.tr (corresponding author)

The phases of QCD are characterized by a variety of condensates in which numerous particles interact with each other through strong forces. The materialization of condensates decreases the energy of a system, and condensates break symmetries in QCD. Chiral symmetry breaking (CSB) is identified by a nonvanishing chiral condensate $\langle\bar{q}q\rangle$, where q is the quark field. Luckily, at extreme temperatures, it is predicted that quark masses are decreased from their effective mass values in hot medium to their bare ones, and CSB is almost restored. Specifically, the condensates, depending on temperature and baryon density, play a key role in the structure of hadrons [37–39].

Recreating longer-lived QGP as well as a large number and assortment of particles in laboratory conditions enables us to explore the properties of QGP and also understand the QCD vacuum, confinement, and hadronization phase of the QGP. For a more precise interpretation of heavy-ion collision experiments, deviations of the hadronic parameters depending on temperature are vital and worth calculating. From the theoretical point of view, these results have delivered some surprising and stimulating new theoretical studies of hot matter [40–42].

Charm and bottom quarks are excellent probes of the hot and dense state of deconfined quarks and gluons. Heavy quarks are created at the initial stages of the hard-scattering collisions and interact with the constituents of the newly produced QGP through both elastic and inelastic processes. These quarks, which can be studied through their decays into leptons, lose energy while propagating through the QGP medium. The formation of a QGP phase also lets them move freely and recombine to produce exotic states. They can coalesce to create standard and possibly exotic bound states at the end of the QGP phase.

On the other hand, although a coherent picture of collision dynamics is emerging, finding signatures of QGP remains a challenge. Verification of QGP formation will probably not come from a unique signal, and evidence based on well-focused observations will have to be collected. Some signatures supporting the creation of the QGP have been reported: suppression (and regeneration) of heavy quarkonia, jet quenching, the nonviscous flow, and radiation of photons and dileptons.

Based on these ideas, the purpose of this article is to evaluate the mass and meson-current coupling constant, and decay width of $Z_{cs}(3985)$ assuming it has four-quark content $[\bar{c}cu\bar{s}]$ including quark, gluon, and quark–gluon mixed condensates up to dimension six using the QCD sum rule (QCDSR) approach at finite temperature. In this case, the vacuum condensate expressions are replaced with their thermal condensates. This analysis can provide some hints regarding the nature of the $Z_{cs}(3985)$ and also provide insights into the nature of the produced hot and dense matter which is predicted to exist in the initial stages of the universe and also in the core of neutron stars [43].

The paper is organized as follows. The thermal QCDSR (TQCDSR) approach employed in our calculations is introduced in Sect. 2. Numerical analysis of the mass and meson-current coupling constant of $Z_{cs}(3985)$ and its b-partner (hereafter referred to as Z_{cs} and Z_{bs} for brevity) is discussed in Sect. 3. In the next section, the decay width of $Z_{cs}(3985)$ is evaluated. After providing a summary in Sect. 5, we present the explicit form of the two-point thermal spectral densities $\rho^{\rm QCD}(s,T)$ obtained from the TQCDSR theory in Appendix A.

2 Theoretical framework for a two-point correlator

The QCDSR technique is a successful and powerful nonperturbative method [44,45] which is widely applied to study the mass spectra and decay properties of hadrons. To find the variations of mass and meson-current coupling of Z_{cs} with increasing temperature, we adopt the QCDSR formalism for TQCDSR. We start the calculation by writing the correlation function [46]:

$$\Pi_{\mu\nu}(q,T) = i\int {\rm d}^4x\, e^{iq\cdot x}\langle\Omega|\mathcal{T}\{\eta_\mu(x)\eta_\nu^\dagger(0)\}|\Omega\rangle, \tag{2}$$

where $\mathcal{T}$ represents the time-ordering operator, Ω signifies the thermal medium, T is the temperature, and $\eta_\mu(x)$ is the interpolating current accompanying resonance Z_{cs}.

To derive the TQCDSR, we start by computing the correlation function in connection with the physical degrees of freedom. The correlation function is expressed by saturation via a complete set of states with the same quantum number $J^P = 1^+$ of the Z_{cs} state, and then Eq. (2) is integrated for x:

$$\Pi_{\mu\nu}^{\rm Phys}(q,T) = \frac{\langle\Omega|\eta_\mu|Z_{cs}(q)\rangle\langle Z_{cs}(q)|\eta_\nu^\dagger|\Omega\rangle}{m_{Z_{cs}}^2(T)-q^2} + \cdots, \tag{3}$$

where $m_{Z_{cs}}(T)$ is the temperature-dependent ground-state mass of axial-vector state Z_{cs}, and three dots indicate the higher states and continuum. The definition of the matrix element of temperature-dependent meson-current coupling constants is

$$\langle\Omega|\eta_\mu|Z_{cs}(q)\rangle = \lambda_{Z_{cs}}(T)m_{Z_{cs}}(T)\varepsilon_\mu, \tag{4}$$

where ε_μ is the polarization vector. Thus the correlation function for the physical side can be written concerning the thermal ground-state mass and meson-current coupling constant in the form below:

$$\Pi_{\mu\nu}^{\rm Phys}(q,T) = \frac{m_{Z_{cs}}^2(T)\,\lambda_{Z_{cs}}^2(T)}{m_{Z_{cs}}^2(T)-q^2}\left(-g_{\mu\nu}+\frac{q_\mu q_\nu}{m_{Z_{cs}}^2(T)}\right) + \cdots. \tag{5}$$

In our computations, the chosen structure for both the physical and QCD parts of the correlator is $(g_{\mu\nu})$ to obtain the TQCDSR for the mass and meson-current coupling constant. Then, isolating ground-state contributions from the higher resonances and continuum states by taking the derivative, namely using Borel transformation, the physical side is determined as

$$\widehat{\mathcal{B}}(q^2)\Pi^{\rm Phys}(q^2,T)=m^2_{Z_{cs}}(T)\lambda^2_{Z_{cs}}(T)\,e^{-m^2_{Z_{cs}}(T)/M^2}, \quad (6)$$

where M is the Borel parameter in the QCDSR model.

The next step is to determine the QCD part in which the correlation function is expressed with the quark and gluon degrees of freedom. First, we choose the concerned current for the Z_{cs} state with $J^P=1^+$ constructed in a tetraquark picture as

$$\eta_\mu(x)=i\epsilon_{abc}\epsilon_{dec}\Big[\big(s^T_a(x)C\gamma_5 c_b(x)\big)\big(\overline{u}_d(x)\gamma_\mu C\overline{c}^T_e(x)\big)\Big], \quad (7)$$

where ϵ_{abc} and ϵ_{dec} are antisymmetric Levi–Civita symbols, a, b, c, d, e are color indices, and C is the charge conjugation matrix.

The QCD part of the correlation function $\Pi^{\rm QCD}_{\mu\nu}(q,T)$ can be described, as usual, with a dispersion integral:

$$\Pi^{\rm QCD}(q^2,T)=\int_{\mathcal{M}^2}^{\infty}\frac{\rho^{\rm QCD}(s,T)}{s-q^2}{\rm d}s, \quad (8)$$

where $\mathcal{M}^2=(m_u+m_s+2m_c)^2$, and the spectral density function $\rho^{\rm QCD}(s,T)$ is given by the imaginary part of the correlation function:

$$\rho^{\rm QCD}(s,T)=\frac{1}{\pi}Im[\Pi^{\rm QCD}]. \quad (9)$$

Having completed lengthy calculations, the QCD side of the correlation function in terms of the heavy and light quark propagators reads

$$\begin{aligned}
&\Pi^{\rm QCD}_{\mu\nu}(q,T)\\
&=-\frac{i}{2}\int {\rm d}^4x e^{iq\cdot x}\epsilon_{abc}\tilde{\epsilon}_{dec}\epsilon'_{a'b'c'}\tilde{\epsilon}'_{d'e'c'}\\
&\times\Big({\rm Tr}[\widetilde{S}^{e'e}_c(-x)\gamma_\nu S^{{\rm d}'d}_u(-x)\gamma_\mu]{\rm Tr}[\widetilde{S}^{aa'}_s(x)\gamma_5 S^{bb'}_c(x)\gamma_5]\\
&-{\rm Tr}[\widetilde{S}^{e'e}_c(-x)\gamma_5 S^{{\rm d}'d}_u(-x)\gamma_\mu]{\rm Tr}[\widetilde{S}^{aa'}_s(x)\gamma_5 S^{bb'}_c(x)\gamma_\nu]\\
&-{\rm Tr}[\widetilde{S}^{e'e}_c(-x)\gamma_\nu S^{{\rm d}'d}_u(-x)\gamma_5]{\rm Tr}[\widetilde{S}^{aa'}_s(x)\gamma_\mu S^{bb'}_c(x)\gamma_5]\\
&+{\rm Tr}[\widetilde{S}^{e'e}_c(-x)\gamma_5 S^{{\rm d}'d}_u(-x)\gamma_5]{\rm Tr}[\widetilde{S}^{aa'}_s(x)\gamma_\mu S^{bb'}_c(x)\gamma_\nu]\Big),
\end{aligned} \quad (10)$$

and for compactness we used the following notation in Eq. (10):

$$\widetilde{S}^{aa'}(x)=CS^{aa'T}(x)\,C.$$

By the way, at finite temperatures, the additional operators arise in the short distance expansion of the product of two quark bilinear operators because of the failure of Lorentz invariance with the preferred reference frame and spilling of the residual $\mathcal{O}(3)$ symmetry, and accordingly the thermal heavy and light quark propagators include new terms. So we modify the vacuum condensates by their thermal averages.

In the calculations, we use the following definition of the thermal light quark propagator $S^{ij}_q(x)$ [47–49]:

$$\begin{aligned}
&S^{ij}_q(x)\\
&=i\frac{\not{x}}{2\pi^2x^4}\delta_{ij}-\frac{m_q}{4\pi^2x^2}\delta_{ij}-\frac{\langle\bar{q}q\rangle_T}{12}\delta_{ij}\\
&-\frac{x^2}{192}m_0^2\langle\bar{q}q\rangle_T\Big[1-i\frac{m_q}{6}\not{x}\Big]\delta_{ij}+\frac{i}{3}\Big[\not{x}\Big(\frac{m_q}{16}\langle\bar{q}q\rangle_T\\
&-\frac{1}{12}\langle u^\mu\theta^f_{\mu\nu}u^\nu\rangle\Big)+\frac{1}{3}(u\cdot x)\not{u}\langle u^\mu\theta^f_{\mu\nu}u^\nu\rangle\Big]\delta_{ij}\\
&-\frac{ig_sG^{\alpha\beta}_{ij}}{32\pi^2x^2}\Big(\not{x}\sigma_{\mu\nu}+\sigma_{\mu\nu}\not{x}\Big)-i\delta_{ij}\frac{x^2\not{x}\langle\bar{q}q\rangle^2_T}{7776}g_s^2,
\end{aligned} \quad (11)$$

where m_q is the light quark mass, $\langle\bar{q}q\rangle_T$ denotes the temperature-dependent light quark condensate, u_μ is the four-velocity of hot matter, and $\theta^f_{\mu\nu}$ is the fermionic part of the energy momentum tensor. Also, the gluon condensate depending on the gluonic part of the energy–momentum tensor $\theta^g_{\lambda\sigma}$ is [49]

$$\begin{aligned}
&\langle Tr^cG_{\alpha\beta}G_{\mu\nu}\rangle\\
&=\frac{1}{24}(g_{\alpha\mu}g_{\beta\nu}-g_{\alpha\nu}g_{\beta\mu})\langle G^a_{\lambda\sigma}G^{a\lambda\sigma}\rangle\\
&+\frac{1}{6}\Big[g_{\alpha\mu}g_{\beta\nu}-g_{\alpha\nu}g_{\beta\mu}-2(u_\alpha u_\mu g_{\beta\nu}-u_\alpha u_\nu g_{\beta\mu}\\
&-u_\beta u_\mu g_{\alpha\nu}+u_\beta u_\nu g_{\alpha\mu})\Big]\langle u^\lambda\theta^g_{\lambda\sigma}u^\sigma\rangle.
\end{aligned} \quad (12)$$

The heavy quark propagator $S^{ij}_Q(x)$ $(Q=c,b)$ is described as in Ref. [49]:

$$\begin{aligned}
S^{ij}_Q(x)=i\int\frac{{\rm d}^4k}{(2\pi)^4}e^{-ik\cdot x}\Big[&\frac{\delta_{ij}\Big(\not{k}+m_Q\Big)}{k^2-m_Q^2}\\
&-\frac{gG^{\alpha\beta}_{ij}}{4}\frac{\sigma_{\alpha\beta}\Big(\not{k}+m_Q\Big)+\Big(\not{k}+m_Q\Big)\sigma_{\alpha\beta}}{(k^2-m_Q^2)^2}\\
&+\frac{g^2}{12}G^A_{\alpha\beta}G^{\alpha\beta}_A\delta_{ij}m_Q\frac{k^2+m_Q\not{k}}{(k^2-m_Q^2)^4}+\cdots\Big],
\end{aligned} \quad (13)$$

where for the external gluon field $G^{\alpha\beta}_{ij}$, the below shorthand notation is employed:

$$G^{\alpha\beta}_{ij}\equiv G^{\alpha\beta}_A\lambda^A_{ij}/2,$$

where λ^{ij}_A are Gell–Mann matrices, i, j are color indices, and $A=1,\,2\ldots 8$ are the number of gluon flavors. The first term in Eq. (13) denotes the perturbative contribution to the heavy quark propagator, and the others are non-perturbative terms.

Then, taking into account the tensor structure of $\Pi_{\mu\nu}^{\rm QCD}(q,T)$ we can write

$$\Pi_{\mu\nu}^{\rm QCD}(q^2,T)=\Pi_0^{\rm QCD}(q^2,T)\frac{q_\mu q_\nu}{q^2}+\Pi_1^{\rm QCD}(q^2,T)\left(-g_{\mu\nu}+\frac{q_\mu q_\nu}{q^2}\right), \quad (14)$$

where $\Pi_0^{\rm QCD}(q^2,T)$ and $\Pi_1^{\rm QCD}(q^2,T)$ are invariant functions. According to the idea of the QCDSR, we should choose the same structures $(g_{\mu\nu})$ for the mass and the meson-current coupling constant sum rules in both $\Pi_{\mu\nu}^{\rm Phys}(q^2,T)$ and $\Pi_{\mu\nu}^{\rm QCD}(q^2,T)$.

Now, using these definitions, transferring the continuum contribution to the QCD part, and applying Borel transformation to both parts of the sum rules and equating them, the thermal meson-current coupling constant sum rule for the axial-vector meson Z_{cs} up to the dimension-six condensates is written as follows:

$$m_{Z_{cs}}^2(T)\,\lambda_{Z_{cs}}^2(T)e^{-m_{Z_{cs}}^2(T)/M^2}=\int_{\mathcal{M}^2}^{s_0(T)}{\rm d}s\rho^{\rm QCD}(s,T)e^{-s/M^2}. \quad (15)$$

And then taking the derivative of Eq. (15) in terms of $(-1/M^2)$, we reach the thermal mass sum rule of Z_{cs}:

$$m_{Z_{cs}}^2(T)=\frac{\int_{\mathcal{M}^2}^{s_0(T)}{\rm d}s s\rho^{\rm QCD}(s,T)e^{-s/M^2}}{\int_{\mathcal{M}^2}^{s_0(T)}{\rm d}s\rho^{\rm QCD}(s,T)e^{-s/M^2}}, \quad (16)$$

where $s_0(T)$ symbolizes the thermal continuum threshold parameter which separates the ground state from higher states. The next step is to carry out the numerical analysis to determine the values of the hadronic parameters of resonance Z_{cs} and also replace the c quark with the b quark to obtain the Z_{cs}'s b-partner Z_{bs} in the tetraquark assumption.

3 Analysis of the mass and meson-current coupling constant of the Z_{cs} and Z_{bs}

To obtain the values of the mass and meson-current coupling constant of the hidden-charm system Z_{cs} in the TQCDSR approach, we require certain parameters, e.g., quark masses, quark, gluon, and mixed vacuum and thermal condensates. The vacuum values of these input parameters are listed in Table 1.

Further, we need temperature-dependent quark, gluon condensates, and energy density as well. Thermal quark condensates are obtained by fitting data from Ref. [50], which is consistent with the lattice QCD data:

$$\frac{\langle\bar{q}q\rangle_T}{\langle 0|\bar{q}q|0\rangle}=\mu_1 e^{c_1 T}+\mu_2, \quad (17)$$

Table 1 Input parameters

Parameters	Values
m_u	$2.16^{+0.49}_{-0.26}$ MeV [51]
m_d	$4.67^{+0.48}_{-0.17}$ MeV [51]
m_s	93^{+11}_{-5} MeV [51]
m_c	1.23 ± 0.09 GeV [51,52]
m_b	$4.18^{+0.03}_{-0.02}$ MeV [51]
$\langle 0\|\bar{q}q\|0\rangle$	$(-275(5))^3$ MeV^3 [50]
$\langle 0\|\bar{s}s\|0\rangle$	$(-296(11))^3$ MeV^3 [50]
$\langle\frac{\alpha_s G^2}{\pi}\rangle$	0.028(3) GeV^4 [53]
m_0^2	(0.8 ± 0.1) GeV^2 [44,45]

where q denotes the u or d quarks, while for the s quark,

$$\frac{\langle\bar{s}s\rangle_T}{\langle 0|\bar{s}s|0\rangle}=\mu_3 e^{c_2 T}+\mu_4. \quad (18)$$

Here, $c_1=0.040\,{\rm MeV}^{-1}$, $c_2=0.516\,{\rm MeV}^{-1}$, $\mu_1=-6.534\times10^{-4}$, $\mu_2=1.015$, $\mu_3=-2.169\times10^{-5}$, and $\mu_4=1.002$ are coefficients [54] and are trustworthy up to a temperature $T=180$ MeV, and $\langle 0|\bar{q}q|0\rangle$ denotes the condensate of the light quarks at $T=0$.

The gluonic and fermionic parts of the energy density can be parametrized as in Ref. [47], taking into account the lattice QCD data given in Ref. [55]:

$$\langle u^\mu\theta_{\mu\nu}^f u^\nu\rangle_T=(\tau_1 e^{c_3 T}+\mu_5)\,T^4, \quad (19)$$

$$\langle u^\mu\theta_{\mu\nu}^g u^\nu\rangle_T=(\tau_2 e^{c_4 T}-\mu_6)\,T^4, \quad (20)$$

where $\tau_1=0.009$, $c_3=24.876\,{\rm GeV}^{-1}$, $\mu_5=0.024$, $\tau_2=0.091$, $c_4=21.277\,{\rm GeV}^{-1}$, and $\mu_6=0.731$ [54].

Also, the temperature-dependent gluon condensate $\langle G^2\rangle_T$ is defined as in Ref. [50]:

$$\delta\left\langle\frac{\alpha_s G^2}{\pi}\right\rangle_T=-\frac{8}{9}[\delta T_\mu^\mu(T)-m_u\delta\langle\bar{u}u\rangle_T-m_d\delta\langle\bar{d}d\rangle_T-m_s\delta\langle\bar{s}s\rangle_T], \quad (21)$$

where the vacuum-subtracted values of the related quantities are employed as

$$\delta f(T)\equiv f(T)-f(0) \quad (22)$$

and

$$\delta T_\mu^\mu(T)=\varepsilon(T)-3p(T), \quad (23)$$

where $p(T)$ is the pressure and $\varepsilon(T)$ is the energy density. Considering recent lattice evaluations [56,57], the fit function of $\delta T_\mu^\mu(T)$ as obtained in Ref. [54] is

$$\frac{\delta T_\mu^\mu(T)}{T^4}=(\mu_7 e^{c_5 T}+\mu_8), \quad (24)$$

with $\mu_7 = 0.020$, $c_5 = 29.412\ \text{GeV}^{-1}$, and $\mu_8 = 0.115$. Moreover, the following expression for the temperature-dependent strong coupling [58,59] is taken into account in the calculations, being $\Lambda_{\overline{MS}} \simeq T_c/1.14$:

$$g_s^{-2}(T) = \frac{11}{8\pi^2}\ln\left(\frac{2\pi T}{\Lambda_{\overline{MS}}}\right) + \frac{51}{88\pi^2}\ln\left[2\ln\left(\frac{2\pi T}{\Lambda_{\overline{MS}}}\right)\right]. \quad (25)$$

As for the temperature-dependent continuum threshold, $s_0(T)$ belonging to the Z_{cs} state is another auxiliary parameter that can be defined as in the following form [60–62]:

$$\frac{s_0(T)}{s_0(0)} = \left(\frac{\langle\bar{q}q\rangle_T}{\langle 0|\bar{q}q|0\rangle}\right)^{2/3}. \quad (26)$$

Continuum threshold parameter $s_0(0)$ is not completely independent of the mass of the first excited state of Z_{cs}. According to the QCDSR formalism, the physical quantities should not be connected with the auxiliary parameters M^2 and s_0. However, M^2 and s_0 are susceptible to the selection of the parameters of the theory.

In the QCDSR method, operator product expansion (OPE) convergence points us to the lower bound on M^2, and the pole contribution (PC) yields the upper bound; i.e., the highest-dimensional condensates should contribute no more than $\sim$ 20% to the QCD side while the continuum is less than 50% of the total terms.

In this context, the maximum allowed M^2 needs be fixed to obey the restriction dictated on PC. At the maximum value of M^2, the constraint PC > 0.2 is typical for multiquark systems, and we obtain

$$\text{PC} = \frac{\Pi(M^2,\ s_0)}{\Pi(M^2,\ \infty)} = 0.24, \quad (27)$$

where $\Pi(M^2,\ s_0)$ is the Borel-transformed and subtracted invariant amplitude $\Pi^{\text{OPE}}(p^2)$.

To ensure the convergence of the OPE, at the minimum limit of M^2 we use the limitation $R \leq 0.15$. The lower bound of the Borel window is defined from the convergence of the OPE by the ratio below:

$$R(M^2) = \frac{\Pi^{(\text{Dim5+Dim6})}(M^2,\ s_0)}{\Pi(M^2,\ s_0)} = 0.15, \quad (28)$$

where Dim5 and Dim6 show the contributions to the correlation function of the sum of the last two terms in the OPE.

Considering all these constraints, according to our analyses, the continuum threshold and Borel parameters are fixed for the Z_{cs} resonance respectively as

$$\begin{aligned} 4\ \text{GeV}^2 &\leq M^2 \leq 5\ \text{GeV}^2, \\ 19.5\ \text{GeV}^2 &\leq s_0 \leq 20.5\ \text{GeV}^2, \end{aligned} \quad (29)$$

and for the Z_{bs} state as well:

$$\begin{aligned} 13\ \text{GeV}^2 &\leq M^2 \leq 15\ \text{GeV}^2, \\ 122\ \text{GeV}^2 &\leq s_0 \leq 126\ \text{GeV}^2. \end{aligned} \quad (30)$$

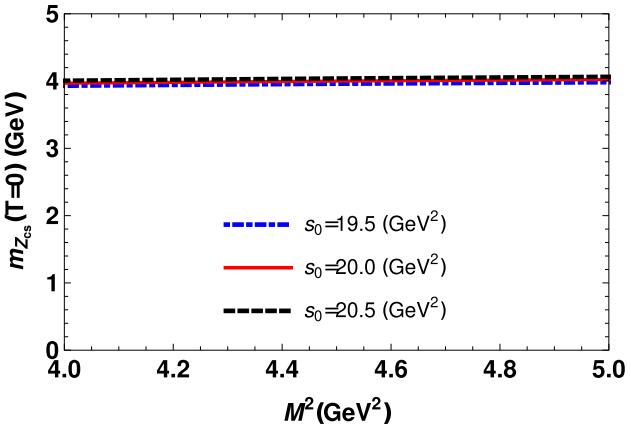

Fig. 1 The vacuum mass of the Z_{cs} state versus Borel parameter M^2 for fixed continuum threshold values in the tetraquark picture

The philosophy of the QCDSR method dictates that the dependence of hadronic quantities on Borel parameter M^2 and continuum threshold s_0 should stay steady in the selected working region. This means that we can obtain reliable results from the extracted sum rules. We see the stability of sum rules according to the model parameters drawing graphs. Here, we only present a plot for the Z_{cs} state in Fig. 1.

In the end, the results obtained for Z_{cs} resonance in the $T = 0$ limit of the TQCDSR model are as follows:

$$\begin{aligned} m_{Z_{cs}} &= 3.996^{+0.068}_{-0.067}\ \text{GeV}, \\ \lambda_{Z_{cs}} &= 0.72^{+0.06}_{-0.05} \times 10^{-2}\ \text{GeV}^4, \end{aligned}$$

whereas we set a range for the state Z_{bs} as

$$\begin{aligned} m_{Z_{bs}} &= (10.379 \sim 10.557)\ \text{GeV}, \\ \lambda_{Z_{bs}} &= (2.73 \sim 3.36) \times 10^{-2}\ \text{GeV}^4, \end{aligned}$$

which is consistent with the experimental and theoretical estimations in Refs. [15–20,23–25] within the limits of uncertainties [14].

Next, we define the modifications of the mass and meson-current coupling constant of the Z_{cs} in terms of temperature. In this manner, graphs showing the ratios of mass and meson current constants with respect to the ratio of T/T_c for the tetraquark assumption are plotted in Figs. 2 and 3, respectively.

4 Strong decays of the tetraquark $Z_{cs}(3985)$

The quark component of the newly observed resonance Z_{cs} should be $[c\bar{c}s\bar{u}]$ rather than the pure $c\bar{c}$ since it is a charged particle with strangeness, and the mass of this tetraquark is large enough to kinematically allow the strong decay modes $D_s^- D^{*0}/D_s^{*-} D^0$. In this part of the paper, we discuss the details of the decays $Z_{cs} \to D_s^- D^{*0}/D_s^{*-} D^0$.

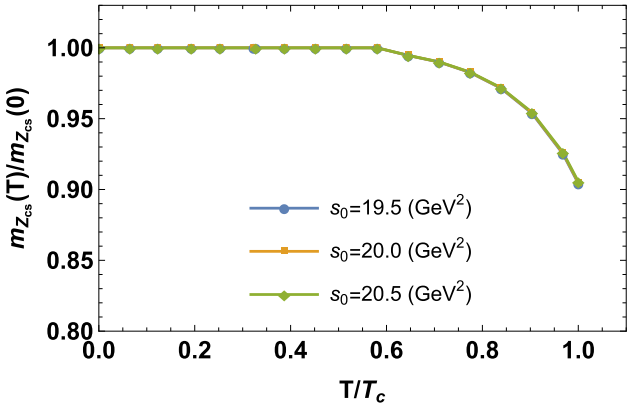

Fig. 2 The ratio of the temperature-dependent mass to vacuum mass of the Z_{cs} state, respectively, in the tetraquark picture for fixed values of $s_0(0)$

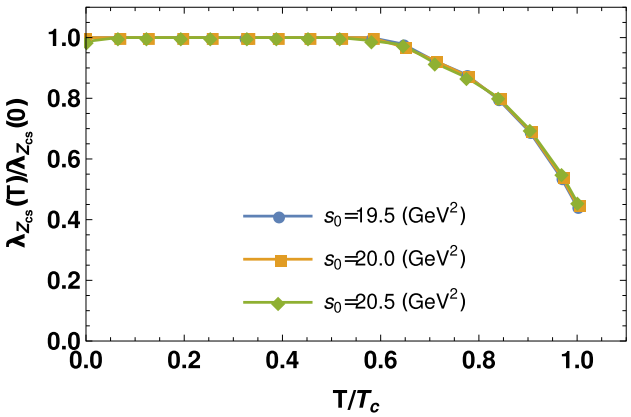

Fig. 3 The ratio of the temperature-dependent meson-current coupling constant to vacuum meson-current coupling constant of the Z_{cs} state, respectively, in the tetraquark picture for fixed values of $s_0(0)$

• We start with the first process $Z_{cs} \to D_s^- D^{*0}$. Initially, we need to compute the strong coupling corresponding to the vertex $Z_{cs}D_s^-D^{*0}$ which quantitatively defines strong interactions between the tetraquark and two conventional mesons. To obtain the QCD three-point sum rules for the related coupling, we begin the calculation by writing the correlation function:

$$\Pi_{\mu\nu}(p,p',T) = i^2 \int \mathrm{d}^4x \mathrm{d}^4y e^{i(p'\cdot y - p\cdot x)} \langle \Omega|\mathcal{T}\{\eta_\nu^{D^{*0}}(y) \times \eta^{D_s^-}(0)\eta_\mu^{Z_{cs}}(x)\}|\Omega\rangle, \quad (31)$$

where $\eta_\mu^{Z_{cs}}(x)$, $\eta^{D_s^-}(0)$, and $\eta_\nu^{D^{*0}}(y)$ represent the interpolating currents for the tetraquark Z_{cs} and mesons D_s^- and D^{*0}, respectively. The four-momenta of the tetraquark Z_{cs} and meson D^{*0} are p and p', respectively, and so the momentum of the meson D_s^- is $q = p - p'$. The current $\eta_\mu^{Z_{cs}}(x)$ is given by Eq. (7) in Sect. 2, while for the remaining two currents we employ

$$\eta_\nu^{D^{*0}}(y) = \bar{u}^g(y) i\gamma_\nu c^g(y), \quad \eta^{D_s^-}(0) = i\bar{c}^f(0)\gamma_5 s^f(0), \quad (32)$$

where g and f are the color indices. Then we apply the standard prescription of the TQCDSR technique and determine the correlation function $\Pi_{\mu\nu}(p,p',T)$ using both physical parameters of the hadrons involved in the process and quark–gluon degrees of freedom. Isolating the ground-state contribution to the correlation function in Eq. (31) from contributions of higher resonances and continuum states for the physical side of the TQCDSR $\Pi_{\mu\nu}^{\mathrm{Phys}}(p,p',T)$, we obtain the following:

$$\Pi_{\mu\nu}^{\mathrm{Phys}}(p,p',T) = \frac{\langle\Omega|\eta_\nu^{D^*}|D^*(p')\rangle\langle\Omega|\eta^{D_s}|D_s(q)\rangle}{(m_{Z_{cs}}^2 - p^2)(m_{D^*}^2 - p'^2)} \times \frac{\langle D_s(q)D^*(p')|Z_{cs}(p)\rangle\langle Z_{cs}(p)|\eta_\mu^{\dagger Z_{cs}}|\Omega\rangle}{(m_{D_s}^2 - q^2)} + \cdots \quad (33)$$

To simplify this expression, we introduce the following matrix elements in terms of the meson's physical parameters:

$$\langle\Omega|\eta_\nu^{D^*}|D^*(p')\rangle = f_{D^*}(T)m_{D^*}(T)\varepsilon'_\nu,$$
$$\langle Z_{cs}(p)|\eta_\mu^{Z_{cs}}|\Omega\rangle = \lambda_{Z_{cs}}(T)m_{Z_{cs}}(T)\varepsilon^*_\mu,$$
$$\langle\Omega|\eta^{D_s}|D_s(q)\rangle = f_{D_s}(T)\frac{m_{D_s}^2(T)}{m_c + m_s}, \quad (34)$$

where $m_{D^*}(T)$, $m_{Z_{cs}}(T)$, $m_{D_s}(T)$ and $f_{D^*}(T)$, $\lambda_{Z_{cs}}(T)$, $f_{D_s}(T)$ are the temperature-dependent masses and decay constants of the mesons $D^*(2007)^0$, $Z_{cs}(3985)$, and $D_s(1968)^-$, respectively. ε'_ν and ε^*_μ are the polarization vectors of the $D^*(2007)^0$ and $Z_{cs}(3985)$ states, respectively. Then we model $\langle D_s(q)D^*(p',s')|Z_{cs}(p,s)\rangle$ in Eq. (34) as follows:

$$\langle D_s(q)D^*(p')|Z_{cs}(p)\rangle = g_1(T)[(p\cdot p') \times(\varepsilon'^*\cdot\varepsilon) - (p\cdot\varepsilon'^*)(p'\cdot\varepsilon)] \quad (35)$$

denoting the strong coupling of the vertex $Z_{cs}(p)D_s(q)D^*(p')$ with $g_1(T)$. Then it is easy to obtain the physical part of the correlation function in Eq. (33):

$$\Pi_{\mu\nu}^{\mathrm{Phys}}(p,p',T) = \frac{g_1(T)f_{D^*}(T)m_{D^*}(T)\lambda_{Z_{cs}}(T)m_{Z_{cs}}(T)}{(m_c+m_s)} \times \frac{f_{D_s}(T)m_{D_s}^2(T)}{(m_{Z_{cs}}^2(T) - p^2)(m_{D^*}^2(T) - p'^2)(m_{D_s}^2(T) - q^2)} \times \left[\frac{m_{Z_{cs}}^2(T) + m_{D^*}^2(T) - m_{D_s}^2(T)}{2} g_{\mu\nu} - p'_\mu p_\nu\right] + \cdots \quad (36)$$

The correlation function $\Pi_{\mu\nu}^{\rm Phys}(p,\,p',\,T))$ contains the two different Lorentz structures proportional to $p'_\mu p_\nu$ and $g_{\mu\nu}$, one of which should be chosen to obtain the sum rules. We select the structure $g_{\mu\nu}$ to work with the invariant amplitude $\Pi^{\rm Phys}(p^2,\,p'^2,\,T)$. We then carry out the double-Borel transformation of this amplitude over variables p^2 and p'^2. This operation allows us to obtain the physical side of the sum rule.

In order to obtain the other side, i.e., the QCD side, of the three-point sum rule, we derive $\Pi_{\mu\nu}(p,\,p',\,T)$ in terms of the quark propagators:

$$\begin{aligned}&\Pi_{\mu\nu}^{\rm QCD}(p,\,p',\,T)\\&=i^4\int {\rm d}^4x{\rm d}^4y e^{i(p'\cdot y-p\cdot x)}\epsilon_{abc}\epsilon_{dec}\\&\times{\rm Tr}[S_c^{ef}(x)\gamma_5 S_s^{fa}(-x)\gamma_5\widetilde{S}_c^{gb}(y-x)\gamma_\nu\widetilde{S}_u^{dg}(x-y)\gamma_\mu].\end{aligned}\tag{37}$$

The correlation function $\Pi_{\mu\nu}^{\rm QCD}(p,\,p',\,T)$ is computed with dimension-six accuracy and has the same Lorentz structures as $\Pi_{\mu\nu}^{\rm Phys}(p,\,p',\,T)$. The double-Borel transformation $\mathcal{B}\Pi^{\rm QCD}(p^2,\,p'^2,\,T)$ reveals the second side of the sum rule. The Borel-transformed and subtracted amplitude $\Pi^{\rm QCD}(p^2,\,p'^2,\,T)$ can be written based on the spectral density $\widetilde{\rho}(s,\,s',\,T)$ which is proportional to the imaginary part of $\Pi^{\rm QCD}(p,\,p',\,T)$,

$$\begin{aligned}&\Pi(\mathbf{M}^2,\,\mathbf{s}_0,\,T)=\int_{\mathcal{M}^2}^{s_0}{\rm d}s\int_{m_c^2}^{s'_0}{\rm d}s'\widetilde{\rho}(s,\,s',\,T)\\&\times e^{-s/M_1^2}e^{-s'/M_2^2},\end{aligned}\tag{38}$$

where $\mathbf{M}^2=(M_1^2,\,M_2^2)$ and $\mathbf{s}_0=(s_0,\,s'_0)$ represent the Borel mass and continuum threshold parameters, respectively. The pair of parameters (M_1, s_0) corresponds to the initial tetraquark's channels, whereas (M_2, s'_0) depicts the final-state meson. $\mathcal{M}=(2m_c+m_s+m_u)$ and $\widetilde{\rho}(s,\,s',\,T)$ are spectral densities computed as the imaginary parts of the corresponding terms in $\Pi_{\mu\nu}^{\rm QCD}(p,\,p',\,T)$. Next, by equating $\mathcal{B}\Pi^{\rm QCD}(p^2,\,p'^2,\,T)$ and Borel transformation of $\Pi^{\rm Phys}(p^2,\,p'^2,\,T)$, and performing continuum subtraction, we determine the sum rule for the coupling $g_1(T)$ as

$$\begin{aligned}g_1(T)=&\frac{2(m_{D_s}^2(T)-q^2)}{f_{D^*}(T)m_{D^*}(T)\lambda_{Z_{cs}}(T)m_{Z_{cs}}(T)f_{D_s}(T)m_{D_s}^2(T)}\\&\times\frac{(m_c+m_s)\Pi(\mathbf{M}^2,\,\mathbf{s}_0,q^2)}{\big(m_{Z_{cs}}^2(T)+m_{D^*}^2(T)-m_{D_s}^2(T)\big)e^{-m_{Z_{cs}}^2/M_1^2}e^{-m_{D^*}^2/M_2^2}}.\end{aligned}\tag{39}$$

Note that the $g_1(T)$ is a function of T and also relies on the Borel and continuum threshold parameters, but is not explicitly specified in Eq. (39) as arguments of g_1. After that, we introduce a new variable $Q^2=-q^2$ and denote the function obtained as $g_1(Q^2)$.

Table 2 Obtained mass and coupling constant values of D mesons at $T=0$ produced in the decays of tetraquark Z_{cs}

Parameters	Numeric values (GeV)
m_{D^0}	$1.861^{+0.063}_{-0.062}$
$m_{D_s^-}$	$1.966^{+0.060}_{-0.059}$
$m_{D^{*0}}$	$2.005^{+0.051}_{-0.050}$
$m_{D_s^{*-}}$	$2.071^{+0.025}_{-0.024}$
f_{D^0}	$0.22^{+0.01}_{-0.01}$
$f_{D_s^-}$	$0.27^{+0.01}_{-0.01}$
$f_{D^{*0}}$	$0.23^{+0.01}_{-0.01}$
$f_{D_s^{*-}}$	$0.27^{+0.01}_{-0.01}$

Table 3 Fit parameters for the mass and meson-current coupling constant of D_s^-, D^{*0}, D_s^{*-}, D^0 and Z_{cs} states

F_n	A_n(GeV)	B_n(GeV)	C_n(GeV)
$m_{D_s^-}$	-1.375×10^{-4}	0.021	1.970
$m_{D^{*0}}$	-1.135×10^{-4}	0.020	2.008
$m_{D_s^{*-}}$	-1.407×10^{-4}	0.020	2.077
$m_{Z_{cs}}$	-2.206×10^{-4}	0.020	4.001
m_{D^0}	-1.198×10^{-4}	0.021	1.865
	A_n(GeV)	B_n(GeV)	C_n(GeV)
$f_{D_s^-}$	-4.370×10^{-5}	0.021	0.271
$f_{D^{*0}}$	-3.068×10^{-5}	0.020	0.190
$f_{D_s^{*-}}$	-3.690×10^{-5}	0.021	0.271
f_{D^0}	-4.170×10^{-5}	0.021	0.224
	A_n(GeV^4)	B_n(GeV)	C_n(GeV^4)
$\lambda_{Z_{cs}}$	-5.769×10^{-4}	0.023	0.007

The sum rule in Eq. (39) includes the temperature dependence of the mass and current coupling belonging to the final mesons, so we need numerical values of these parameters. Therefore, they are computed with the standard sum rule method, and findings in vacuum are given in Table 2.

The following is the function that best fits the graphs we have drawn for the temperature dependencies of the mass and couplings:

$$F_n(T)=A_n{\rm e}^{\frac{T}{B_n}}+C_n,\tag{40}$$

where F_n, A_n, B_n, and C_n are the fitting parameters. Numerical analysis lets us fix these parameters as in Table 3.

Then, to continue the evaluation of $g_1(Q^2)$, we need to determine $\mathbf{M}^2$ and $\mathbf{s}_0$. The limitations imposed on these auxiliary parameters have been mentioned before. The working region for the Borel mass and continuum threshold is the same range used in the mass and meson-current coupling

constant calculation. The decay width of the considered process should be computed using the strong coupling at the D_s^- meson's mass shell $Q^2 = -m_{D_s}^2$, which is not accessible to the sum rule calculations. We avoid this problem by adopting a fitting procedure using the fit function below:

$$g_{fit}(Q^2) = \frac{g_0}{1 - a\frac{Q^2}{m_{Z_{cs}}^2} + b\left(\frac{Q^2}{m_{Z_{cs}}^2}\right)^2} \tag{41}$$

where $g_0 = 0.22,\ a = -1.37,\ b = -0.84$ are the fit coefficients for the coupling g_1 which gives at the mass shell $Q^2 = -m_{D_s}^2$ in vacuum

$$g_1(-m_{D_s}^2) = 0.36 \pm 0.02\ \text{GeV}^{-1}. \tag{42}$$

The decay width of $Z_{cs} \to D_s^- D^{*0}$ is extracted by the following expression:

$$\begin{aligned}\Gamma_1\left[Z_{cs} \to D_s^- D^*(2007)^0\right] &= \frac{g_1^2(T) m_{D^*}^2(T)}{24\pi} \times \xi(m_{Z_{cs}}(T), m_{D^*}(T), m_{D_s^-}(T)) \\ &\times\left[3 + \frac{2\xi^2(m_{Z_{cs}}(T), m_{D^*}(T), m_{D_s^-}(T))}{m_{D^*}^2(T)}\right],\end{aligned} \tag{43}$$

where

$$\xi(a,b,c) = \frac{1}{2a}\sqrt{a^4 + b^4 + c^4 - 2(a^2b^2 + a^2c^2 + b^2c^2)}. \tag{44}$$

Employing the vacuum value of strong coupling from Eq. (42) and the m_{D^*} from Table 2, the decay width of $Z_{cs} \to D_s^- D^*(2007)^0$ is

$$\Gamma_1\left[Z_{cs} \to D_s^- D^*(2007)^0\right] = (4.35 \pm 0.44)\ \text{MeV}. \tag{45}$$

• The second process $\widetilde{Z}_{cs} \to D_s^{*-} D^0$ can be handled in the same way as the first process. Here, however, we utilize the current expressions for the D^0 and D_s^{*-} mesons

$$\eta_\nu^{D^0}(y) = i\bar{u}^g(y)\gamma_5 c^g(y),\ \eta^{D_s^{*-}}(0) = \bar{c}^f(0)\gamma_\nu s^f(0), \tag{46}$$

and we introduce the new matrix elements:

$$\begin{aligned}\langle\Omega|\eta^{D^0}|D^0(p')\rangle &= \frac{f_{D^0}(T) m_{D^0}^2(T)}{m_c}, \\ \langle Z_{cs}(p)|\eta_\mu^{Z_{cs}}|\Omega\rangle &= \lambda_{Z_{cs}}(T)\, m_{Z_{cs}}(T)\, \varepsilon_\mu^*, \\ \langle\Omega|\eta_\nu^{D_s^*}|D_s^*(q,\varepsilon')\rangle &= f_{D_s^*}(T)\, m_{D_s^*}(T)\, \varepsilon_\nu'.\end{aligned} \tag{47}$$

By applying the standard procedures mentioned above for the first process, $\widetilde{\Pi}^{\text{Phys}}(p, p', T)$ and $\widetilde{\Pi}^{\text{OPE}}(p, p', T)$ yield the sum rule

$$\begin{aligned}g_2(q^2) &= \frac{(m_{D_s^*}^2(T) - q^2)}{f_{D^0}(T) m_{D^0}^2(T) \lambda_{Z_{cs}}(T) m_{Z_{cs}}(T) f_{D_s^*}(T) m_{D_s^*(T)}} \\ &\times \frac{2m_c \widetilde{\Pi}(\mathbf{M}^2, \mathbf{s}_0, q^2)}{\left(m_{Z_{cs}}^2(T) + m_{D_s^*}^2(T) - m_{D^0}^2(T)\right) e^{-m_{Z_{cs}}^2/M_1^2} e^{-m_{D^0}^2/M_2^2}}.\end{aligned} \tag{48}$$

Selecting the auxiliary parameters according to the same criteria as stated above, and to determine the coupling constant g_2 at $T = 0$, employing the fit function in Eq. (41) with coefficients $g_0 = 0.24,\ a = -1.52$, and $b = -0.92$ at the mass shell $Q^2 = -m_{D_s^*}^2$ reads:

$$g_2(-m_{D_s^*}^2) = 0.47 \pm 0.03\ \text{GeV}^{-1}. \tag{49}$$

The decay width of the second process is defined by the formula

$$\begin{aligned}\Gamma_2[\widetilde{Z}_{cs} \to D_s^{*-} D^0] &= \frac{g_2^2(T) m_{D_s^{*-}}^2(T)}{24\pi} \times \xi\left(m_{\widetilde{Z}_{cs}}(T), m_{D_s^{*-}}(T), m_{D^0}(T)\right) \\ &\times\left(3 + \frac{2\left[\xi(m_{\widetilde{Z}_{cs}}(T), m_{D_s^{*-}}(T), m_{D^0}(T))\right]^2}{m_{D_s^{*-}}^2(T)}\right),\end{aligned} \tag{50}$$

and our prediction for this decay channel is

$$\Gamma_2[\widetilde{Z}_{cs} \to D_s^{*-} D^0] = (7.65 \pm 0.67)\ \text{MeV}. \tag{51}$$

As a result, we obtain the partial widths of these decays in the present section, and using Eqs. (45) and (51), the full width and mean lifetime of Z_{cs} are predicted as

$$\begin{aligned}\Gamma^{\text{full}} &= (12.0 \pm 0.8)\ \text{MeV}, \\ \tau &= (5.5 \pm 0.5) \times 10^{-19}\ \text{s}.\end{aligned} \tag{52}$$

Our result for the Γ^{full} is consistent with the measured value in BESIII [14].

The last step is to analyze the variation in the partial decay widths in terms of temperature. We draw the $\Gamma_{Z_{cs}}(T)/\Gamma_{Z_{cs}}(0)$ versus T/T_c in Fig. 4. As seen from this figure, the decay width is dramatically increased with increasing temperature.

5 Summary and results

Collisions of heavy ions in laboratory conditions allow us to create and investigate the strongly interacting matter in hot medium. Many facilities contribute to probing both the chiral and the deconfinement phase transition from hadronic matter to the QGP and mapping out different domains of the QCD phase diagram. Among these experiments, Relativistic Heavy Ion Collider (RHIC) and Large Hadron Collider (LHC) energies form deconfined matter characterized by vanishing baryon densities and high temperatures consistent with lattice data. Mapping out the region of a first-order transition at large chemical potential is a primary aim of current and upcoming experimental programs. Recently, RHIC

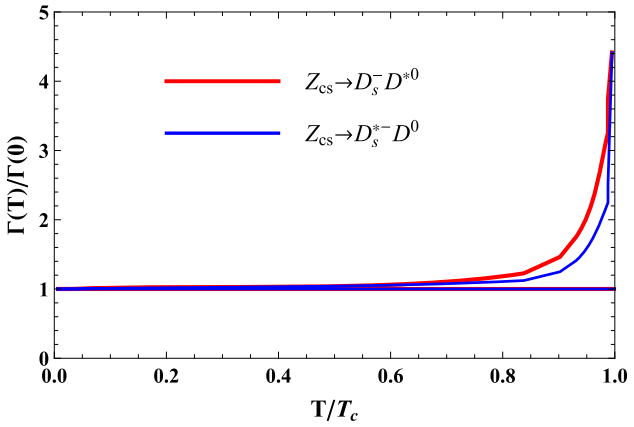

Fig. 4 Variation in the ratio of temperature-dependent decay width of $Z_{cs} \to D_s^- D^{*0}/D_s^{*-} D^0$ to its value in vacuum according to T/T_c for $T_c = 155$ MeV

and LHC have radically increased the energy levels that can be attained by heavy nuclei collisions at near-light speeds, bringing them in line with those of the conditions in the early universe. In addition to these improvements, future experiments at the Facility for Antiproton and Ion Research (FAIR) and at the Nuclotron-based Ion Collider (NICA) will generate a wealth of data.

Also, the ALICE experiment at the CERN LHC finalized a major upgrade and restarted its operations in 2022 with a new computing system in order to handle a data volume roughly 100 times as large as that during the previous operational period. Further constraints can be set by future higher-precision measurements during run 3. The LHC Committee review of the ALICE 3 plans has begun and is expected to be concluded in March 2022 and to deliver highly meaningful physics results.

However, in heavy-ion collisions, the QGP lifetime is ($\sim$ 10 fm/c), and the hadrons would be erased from the spectrum in an extremely short time, as seen from Eq. (52). Hence, it is almost impossible to work with a literally external probe in these collisions, whereas a hadron would continue to exist, albeit with changing mass in QGP medium. Alternatively, such an imaging method can be performed using particles produced during the parton–parton scatterings. Therefore, searching for the signals of QGP provide knowledge to quantitatively understand the charmonium/bottomonium suppression of both conventional and exotic states [63–65] in heavy-ion collisions at high temperatures. This issue may be one of the focus areas of research regarding QGP signals in the near future.

Meanwhile, the newly observed resonance $Z_{cs}(4000)$ with strangeness by the LHCb collaboration led people to wonder whether it was the same state as the $Z_{cs}(3985)$. However, according to our lifetime calculation of $Z_{cs}(3985)$ detected in BESIII, it has a narrower state than the $Z_{cs}(4000)$ in LHCb, and thus they should be different states. This can be tested in future experiments and distinguish the two-state interpretation from the one-state scheme.

In this work, we propose a novel picture, namely thermal QCDSR, to understand the nature of $Z_{cs}(3985)$ with $J^P = 1^+$, and we also reduce our results to $T = 0$ to compare then with experimental and theoretical data in the literature. Additionally, we estimate the hadronic parameters of the b-partner of $Z_{cs}(3985)$, which we hope will be experimentally detected in the near future. According to our numerical evaluations, changes in mass and meson-current coupling constant values are fixed up to $T \cong 100$ MeV, but both start to decrease after this point. At the critical transition temperature, the values of the mass and meson-current coupling constant of $Z_{cs}(3985)$ change up to 10% and 66% , respectively. The thermal width of the $Z_{cs}(3985)$ meson (see Fig. 4) exhibits an increase by roughly a factor of 4.6 near T_c.

As a result, by looking at the numerical analysis, we find that the resonance $Z_{cs}(3985)$ can be well defined as a diquark-antidiquark candidate with quark content $[\bar{c}cu\bar{s}]$. The variations in decay width of $Z_{cs}(3985)$ will provide valuable input to our understanding of the heavy quark system in heavy-ion collisions. However, XYZ exotic states should be tested in more precise experimental data in the future, and we need more experimental studies on the dominant decay channels of $Z_{cs}(3985)$ to elucidate its inner configuration.

Data Availability Statement This manuscript has no associated data or the data will not be deposited. [Authors' comment: All the numerical and mathematical data have been included in the paper and we have no other data regarding this paper.]

Funded by SCOAP[3].

Appendix A: Thermal spectral density functions

In this part, the results of our evaluations for the spectral density are presented for the mass and meson-current coupling constant as a function of the temperature belonging to the $Z_{cs}(3985)$ resonance in the tetraquark picture using the following abbreviations, with Θ as the step function (for brevity, we do not give the spectral density belonging to the decay width here):

$$
\begin{aligned}
L(s,x) &= sx(1-x)-m_c^2,\\
L^{'}(s,x_1,x_2) &= -\frac{(-1+x_2)\Big[-sx_1x_2(-1+x_1+x_2)+m_c^2(x_1+x_2)(x_1^2+x_1(-1+x_2)+(-1+x_2)x_2)\Big]}{(x_1^2+x_1(-1+x_2)+(-1+x_2)x_2)^2},\\
\alpha &= x_1^2+x_1(x_2-1)+x_2(x_2-1),\\
\beta &= x_1+x_2-1,\\
\zeta &= x_1(x_1-1)+x_2(x_1-1)+x_2^2,\\
\eta &= x_1+x_2.
\end{aligned}
$$

We also separate the thermal spectral density functions in terms of dimensions:

$$
\begin{aligned}
\rho^{\rm QCD}(s,T) &= \rho^{\rm pert.}(s)+\rho^{\langle\bar{q}q\rangle}(s,T)+\rho^{G^2+\langle\theta_{00}\rangle}(s,T)\\
&\quad+\rho^{\langle qGq\rangle}(s,T)+\rho^{\langle\bar{q}q\rangle^2}(s,T). \qquad \text{(A1)}
\end{aligned}
$$

The explicit form of spectral densities is performed with the integrals over the Feynman parameters x, x_1, x_2,, and x_3 as follows:

$$
\begin{aligned}
&\rho^{\rm pert}(s)\\
&=-\int_0^1 {\rm d}x_1\int_0^{1-x_1}\frac{{\rm d}x_2}{3072\alpha^8\beta\pi^6}\\
&\times\Big\{\Big(-\alpha\eta m_c^2+\beta s x_1x_2\Big)^2\Big(12\alpha^3\eta m_c^3m_s x_2\\
&+3\alpha^2\eta^2m_c^4x_1x_2-48\alpha^2\beta m_cm_s s x_1x_2^2\\
&-26\alpha\beta\eta m_c^2sx_1^2x_2^2+35\beta^2s^2x_1^3x_2^3\Big)\Big\}\\
&\times\Theta[L^{'}(s,x_1,x_2)], \qquad \text{(A2)}\\
&\rho^{\langle\bar{q}q\rangle}(s,T)\\
&=\int_0^1 {\rm d}x_1\int_0^{1-{\rm d}x_1}\frac{{\rm d}x_2}{64\alpha^6\pi^4}\Big\{15\beta^3m_ss^2\langle\bar{s}s\rangle x_1^3x_2^3\\
&-2\alpha^3\eta^2m_c^5\Big(2\langle\bar{u}u\rangle x_1+\langle\bar{s}s\rangle x_2\Big)\\
&+4\alpha^2\beta\eta m_c^3sx_1x_2\Big(3\langle\bar{u}u\rangle x_1+2\langle\bar{s}s\rangle x_2\Big)\\
&-2\alpha\beta^2m_cs^2x_1^2x_2^2\Big(4\langle\bar{u}u\rangle x_1+3\langle\bar{s}s\rangle x_2\Big)\\
&+4\alpha\beta m_c^2m_ssx_1x_2\Big(-4\beta\eta\langle\bar{s}s\rangle x_1x_2+\langle\bar{u}u\rangle\zeta^2\Big)\\
&-\alpha^2\eta m_c^4m_s\times\Big(-3\beta\eta\langle\bar{s}s\rangle x_1x_2+4\langle\bar{u}u\rangle\zeta^2\Big)\Big\}\\
&\times\Theta[L^{'}(s,x_1,x_2)], \qquad \text{(A3)}\\
&\rho^{G^2+\langle\theta_{00}\rangle}(s,T)\\
&=\int_0^1 {\rm d}x_1\int_0^{1-x_1}{\rm d}x_2\Big\{\frac{1}{2304\alpha^6\beta\pi^6}\Big[3\beta x_2\\
&\times\Big[4\alpha^3\eta m_c^3m_s\Big(8\beta\pi^2\langle u^\mu\theta^f_{\mu\nu}u^\nu\rangle+g_s^2\langle u^\mu\theta^g_{\mu\nu}u^\nu\rangle x_1\Big)\\
&+\alpha^2\eta^2m_c^4x_1\times\Big(64\beta\pi^2\langle u^\mu\theta^f_{\mu\nu}u^\nu\rangle+g_s^2\langle u^\mu\theta^g_{\mu\nu}u^\nu\rangle\\
&\times(3x_1-x_2)\Big)-8\alpha^2\beta m_cm_ssx_1\Big(16\beta\pi^2\langle u^\mu\theta^f_{\mu\nu}u^\nu\rangle\\
&+g_s^2\langle u^\mu\theta^g_{\mu\nu}u^\nu\rangle x_1\Big)x_2-4\alpha\beta\eta m_c^2sx_1^2\\
&\times\Big(208\beta\pi^2\langle u^\mu\theta^f_{\mu\nu}u^\nu\rangle+g_s^2\langle u^\mu\theta^g_{\mu\nu}u^\nu\rangle\\
&\times(4x_1-5x_2)\Big)x_2+5\beta^2s^2x_1^3\Big(192\beta\pi^2\langle u^\mu\theta^f_{\mu\nu}u^\nu\rangle+g_s^2\\
&\times\langle u^\mu\theta^g_{\mu\nu}u^\nu\rangle(3x_1-5x_2)\Big)x_2^2\Big]+\langle\frac{\alpha_sGG}{\pi}\Big\rangle\pi^2\\
&\times\Big[15\beta^3s^2x_1^3(5x_1-9x_2)x_2^3-12\alpha\beta m_cm_ssx_1x_2^2\\
&\times\Big(4(-1+x_1)^2x_1^2+4(-1+x_1)x_1(-1+2x_1)x_2\\
&+7(-1+x_1)x_1x_2^2+(-1+3x_1)x_2^3+x_2^4\Big)\\
&+3\alpha^2m_c^3\Big(m_s(-1+x_1)x_1^3(-12\\
&+13x_1)x_2+m_s(-1+x_1)x_1^2(-24+37x_1)x_2^2\\
&+m_sx_1\Big(12+x_1(-59+48x_1)\Big)x_2^3\\
&+m_sx_1(-25+34x_1)x_2^4+m_s(-2+13x_1)x_2^5+2m_sx_2^6\Big)\\
&+3\alpha^2\eta^2m_c^4x_1x_2\Big(10x_1^2+(9-8x_2)x_2-x_1(9+x_2)\Big)\\
&-8\alpha\beta\eta m_c^2sx_1^2x_2^2\\
&\times\Big(13x_1^2+(18-17x_2)x_2-x_1(12+7x_2)\Big)\Big]\Big]\Big\}\\
&\times\Theta[L^{'}(s,x_1,x_2)], \qquad \text{(A4)}\\
&\rho^{\langle qGq\rangle}(s,T)\\
&=\frac{m_c^2m_o^2m_s\langle\bar{u}u\rangle}{64\pi^4}+\int_0^1{\rm d}x_1\int_0^{1-x_1}{\rm d}x_2\Big\{-\frac{\beta m_o^2}{192\alpha^5\pi^4}\\
&\times\Big[-3\alpha\beta\eta m_c^2m_s\langle\bar{s}s\rangle x_1x_2+8\beta^2m_ss\langle\bar{s}s\rangle x_1^2x_2^2\\
&+3\alpha^2\eta m_c^3\Big(2\langle\bar{u}u\rangle x_1+\langle\bar{s}s\rangle x_2\Big)\\
&-3\alpha\beta m_csx_1x_2\Big(3\langle\bar{u}u\rangle x_1+2\langle\bar{s}s\rangle x_2\Big)\Big]\Big\}\Theta[L^{'}(s,x_1,x_2)], \qquad \text{(A5)}\\
&\rho^{\langle\bar{q}q\rangle^2}(s,T)\\
&=\frac{1}{1296\pi^4}\Big[\int_0^1{\rm d}x\Big\{-108m_c^2\pi^2\langle\bar{s}s\rangle\langle\bar{u}u\rangle+m_cm_s\langle\bar{u}u\rangle
\end{aligned}
$$

$$\times\left(g_s^2\langle\bar{u}u\rangle(-1+x)+108\pi^2\langle\bar{s}s\rangle x\right)\Bigg\}\Theta[L(s,x)]$$
$$+\int_0^{1-x_1}\mathrm{d}x_1\int_0^{1-x_1-x_2}\mathrm{d}x_2\Bigg\{\beta^2 g_s^2\left[\langle\bar{s}s\rangle^2+\langle\bar{u}u\rangle^2\right]x_1x_2$$
$$\times(3\alpha\eta m_c^2-8\beta s x_1x_2)\Bigg\}\Bigg]\Theta[L^{'}(s,x_1,x_2)]. \quad \text{(A6)}$$

References

1. N. Brambilla, S. Eidelman, C. Hanhart, A. Nefediev, C.P. Shen, C.E. Thomas, A. Vairo, C.Z. Yuan, Phys. Rep. **873**, 1–154 (2020)
2. Y.R. Liu, H.X. Chen, W. Chen, X. Liu, S.L. Zhu, Prog. Part. Nucl. Phys. **107**, 237–320 (2019)
3. E. Veli Veliev, S. Günaydın, H. Sundu, Eur. Phys. J. Plus **133**(4), 139 (2018)
4. K. Azizi, N. Er, Phys. Rev. D **101**(7), 074037 (2020)
5. I.B. Işık, H. Sundu, E.V. Veliev, Eur. Phys. J. Plus **135**(1), 48 (2020)
6. H.X. Chen, W. Chen, X. Liu, S.L. Zhu, Phys. Rep. **639**, 1–121 (2016)
7. K. Azizi, N. Er, Phys. Lett. B **811**, 135979 (2020)
8. S.S. Agaev, K. Azizi, H. Sundu, Phys. Rev. D **93**(7), 074002 (2016)
9. S.S. Agaev, K. Azizi, H. Sundu, Phys. Rev. D **96**(3), 034026 (2017)
10. S.S. Agaev, K. Azizi, H. Sundu, Eur. Phys. J. C **77**(12), 836 (2017)
11. S.S. Agaev, K. Azizi, H. Sundu, Turk. J. Phys. **44**(2), 95 (2020)
12. U. Ozdem, K. Azizi, Phys. Rev. D **96**(7), 074030 (2017)
13. H. Sundu, Süleyman Demirel Univ. J. Nat. Appl. Sci. **20**(3), 448–455 (2016)
14. M. Ablikim et al. (BESIII), Phys. Rev. Lett. **126**(10), 102001 (2021)
15. Z.F. Sun, C.W. Xiao, arXiv:2011.09404 [hep-ph]
16. M.C. Du, Q. Wang, Q. Zhao, arXiv:2011.09225 [hep-ph]
17. R. Chen, Q. Huang, Phys. Rev. D **103**(3), 034008 (2021)
18. J.Z. Wang, Q.S. Zhou, X. Liu, T. Matsuki, Eur. Phys. J. C **81**(1), 51 (2021)
19. L. Meng, B. Wang, S.L. Zhu, Eur. Phys. J. C **81**(1), 51 (2021)
20. M.Z. Liu, J.X. Lu, T.W. Wu, J.J. Xie, L.S. Geng, arXiv:2011.08720 [hep-ph]
21. B.D. Wan, C.F. Qiao, Nucl. Phys. B **968**, 115450 (2021)
22. Q.N. Wang, W. Chen, H.X. Chen, Chin. Phys. C **45**(9), 093102 (2021)
23. K. Azizi, N. Er, Eur. Phys. J. C **81**(1), 61 (2021)
24. Z.G. Wang, Chin. Phys. C **45**(7), 073107 (2021)
25. X. Jin, Y. Wu, X. Liu, Y. Xue, H. Huang, J. Ping and B. Zhong, Eur. Phys. J. C **81**(12), 1108 (2021)
26. A. Ayala, S. Hernandez-Ortiz, L.A. Hernandez, V. Knapp-Perez, R. Zamora, Phys. Rev. D **101**(7), 074023 (2020)
27. A. Ayala, C.A. Dominguez, M. Loewe, Adv. High Energy Phys. **2017**, 9291623 (2017)
28. W.J. Fu, J.M. Pawlowski, F. Rennecke, Phys. Rev. D **101**(5), 054032 (2020)
29. J. Zhao, S. Shi, P. Zhuang, Phys. Rev. D **102**(11), 114001 (2020)
30. N. Irikura, H. Saito, Phys. Rev. Res. **2**, 013284 (2020)
31. Y. Aoki, Z. Fodor, S.D. Katz, K.K. Szabo, Phys. Lett. B **643**, 46 (2006)
32. A. Andronic, P. Braun-Munzinger, K. Redlich, J. Stachel, Nature **561**(7723), 321 (2018)
33. P. Steinbrecher (HotQCD Collaboration), Nucl. Phys. A **982**, 847 (2019)
34. C.S. Fischer, Prog. Part. Nucl. Phys. **105**, 1–60 (2019)
35. S. Acharya et al. (ALICE), Nucl. Phys. A **971**, 1–20 (2018)
36. M. Floris, Nucl. Phys. A **931**, 103–112 (2014)
37. T. Hatsuda, Y. Koike, S.H. Lee, Nucl. Phys. B **394**, 221 (1993)
38. P. Foka, M.A. Janik, Rev. Phys. **1**, 154–171 (2016)
39. E.L. Bratkovskaya, A. Palmese, W. Cassing, E. Seifert, T. Steinert, P. Moreau, J. Phys. Conf. Ser. **878**(1), 012018 (2017)
40. P. Lerambert-Potin, J.A. de Freitas Pacheco, Universe **7**(8), 304 (2021)
41. J. Grefa, J. Noronha, J. Noronha-Hostler, I. Portillo, C. Ratti, R. Rougemont, Phys. Rev. D **104**(3), 034002 (2021)
42. S. Pinkanjanarod, P. Burikham, Eur. Phys. J. C **81**(8), 705 (2021)
43. G. Baym, T. Hatsuda, T. Kojo, P.D. Powell, Y. Song, T. Takatsuka, Rep. Prog. Phys. **81**(5), 056902 (2018)
44. M.A. Shifman, A.I. Vainshtein, V.I. Zakharov, Nucl. Phys. B **147**, 385 (1979)
45. L.J. Reinders, H. Rubinstein, S. Yazaki, Phys. Rep. **127**, 1 (1985)
46. A.I. Bochkarev, M.E. Shaposhnikov, Nucl. Phys. B **268**, 220 (1986)
47. K. Azizi, G. Bozkır, Eur. Phys. J. C **76**(10), 521 (2016)
48. K. Azizi, A. Türkan, E. Veli Veliev, H. Sundu, Adv. High Energy Phys. **2015**, 794243 (2015)
49. S. Mallik, Phys. Lett. B **416**, 373 (1998)
50. P. Gubler, D. Satow, Prog. Part. Nucl. Phys. **106**, 1 (2019)
51. P.A. Zyla et al. (Particle Data Group), Prog. Theor. Exp. Phys. **2020**, 083C01 (2020) and 2021 update
52. M. Eidemuller, M. Jamin, Phys. Lett. B **498**, 203–210 (2001)
53. R. Horsley, G. Hotzel, E.M. Ilgenfritz, R. Millo, H. Perlt, P.E.L. Rakow, Y. Nakamura, G. Schierholz, A. Schiller, Phys. Rev. D **86**, 054502 (2012)
54. K. Azizi, A. Türkan, Eur. Phys. J. C **80**(5), 425 (2020)
55. M. Cheng et al., Phys. Rev. D **77**, 014511 (2008)
56. A. Bazavov et al. (HotQCD), Phys. Rev. D **90**, 094503 (2014)
57. S. Borsanyi, Z. Fodor, C. Hoelbling, S.D. Katz, S. Krieg, K.K. Szabo, Phys. Lett. B **730**, 99–104 (2014)
58. O. Kaczmarek, F. Karsch, F. Zantow, P. Petreczky, Phys. Rev. D **70**, 074505 (2004) [Erratum: Phys. Rev. D **72**, 059903 (2005)]
59. K. Morita, S.H. Lee, Phys. Rev. C **77**, 064904 (2008)
60. S. Borsanyi et al. (Wuppertal-Budapest Collaboration), JHEP **1009**, 073 (2010)
61. C.A. Dominguez, L.A. Hernandez, Mod. Phys. Lett. A **31**(36), 1630042 (2016)
62. T. Bhattacharya et al., Phys. Rev. Lett. **113**(8), 082001 (2014)
63. B. Chen, L. Jiang, X. H. Liu, Y. Liu and J. Zhao, Phys Rev C.**105** 054901 (2022)
64. L.M. Abreu, K.P. Khemchandani, A. Martinez Torres, F.S. Navarra, M. Nielsen, Phys. Lett. B **761**, 303–309 (2016)
65. L.M. Abreu, F.S. Navarra, M. Nielsen, A.L. Vasconcellos, Eur. Phys. J. C **78**(9), 752 (2018)